



Supporting Online Material for

Preserved Feedforward but Impaired Top-Down Processes in the Vegetative State

Melanie Boly,* Marta Isabel Garrido, Olivia Gosseries, Marie-Aurélie Bruno, Pierre Boveroux, Caroline Schnakers, Marcello Massimini, Vladimir Litvak, Steven Laureys, Karl Friston

*To whom correspondence should be addressed. E-mail: mboly@ulg.ac.be

Published 13 May 2011, *Science* **332**, 858 (2011)
DOI: 10.1126/science.1202043

This PDF file includes

Materials and Methods
SOM Text
Fig. S1
Table S1
References

Supplementary Online Material

Supplementary methods

Patients

We compared 22 healthy volunteers (age range 20-81 years, mean age $37 \pm$ SD 19 years, 7 males) with 21 brain damaged patients (13 MCS, 8 VS, age range 16-83 years, mean age $48 \pm$ SD 20 years, 12 males). Patients' data are reported in the Supplementary Table. To ensure the generalizability of our results, we included patients with different etiologies and clinical histories, in the hope of finding a common deficit that underlies changes in conscious level, irrespective of its distal causes. Data were acquired in an un-sedated condition. The study was approved by the Ethics Committee of the Medical School of the University of Liège. Informed consent to participate in the study was obtained from the subjects themselves in the case of healthy subjects, and from the legal surrogate for the patients.

Behavioral assessments of consciousness were performed by trained and experienced neuropsychologists using the French adaptation of the Coma Recovery Scale-Revised (CRS-R) (S1-2) that has been specifically developed to disentangle VS from MCS patients but also MCS patients from patients who recovered their ability to communicate functionally (EMCS). The scale comprises six subscales: auditory, visual, motor and oromotor/verbal functions, as well as communication and level of arousal (see Supplementary Table for scores obtained by each patient in the CRS-R subscales). The 23 items are ordered according to their degree of complexity; the lowest item on each subscale represents reflexive activity, while the highest item represents behaviors that are cognitively mediated. Scoring is based on the presence or absence of operationally-defined behavioral responses to specific sensory stimuli (e.g., if visual pursuit of a mirror is present at least two times in the same direction, the patient is then considered to be MCS).

Data acquisition

We recorded auditory evoked potentials using a 60-channel EEG amplifier (Nexstim Ltd, Helsinki FI) (S3). To optimize signal quality, the impedance at all electrodes was kept below 5 k Ω . EEG signals were referenced to an additional electrode on the forehead, filtered (0.1-

500 Hz) and sampled at 1450 Hz. Two extra sensors were used to record the electro-oculogram (EOG). To avoid a confounding effect due to differences in vigilance, arousal was maintained at a constant level throughout the experiment. During each EEG session, patients were lying on their beds, awake and with their eyes open. If signs of drowsiness appeared, recordings were momentarily interrupted and subjects were stimulated using the CRS-R arousal facilitation protocols. At the end of the experiment, the electrode positions and scalp landmarks (nasion, right and left tragus) were digitized.

Electroencephalographic activity was measured during an auditory roving ‘oddball’ paradigm (see Fig. 1A). The stimuli comprised a structured sequence of pure sinusoidal tones, with a roving, or sporadically changing tone. This paradigm is similar to that used in previous DCM studies investigating the functional architecture of mismatch negativity response (MMN) in healthy volunteers (S4-5). Within each stimulus train, all tones were of one frequency and were followed by a train of a different frequency. The first tone of a train was a deviant, which eventually became a standard after few repetitions. This paradigm ensures that deviants and standards have exactly the same physical properties, differing only in the number of times they have been presented. This was varied pseudo-randomly between one and eleven. The probability that the same one was presented once or twice was 2.5%; for three and four times the probability was 3.75% and for five to eleven times it was 12.5%. The frequency of the tones varied from 500 to 800 Hz, in random steps with integer multiples of 50 Hz. Stimuli were presented binaurally via headphones for 15 min. The duration of each tone was 70 ms, with 5ms rise and fall times, and the inter-stimulus interval was 500 ms. About 250 deviant trials (first tone) and about 200 standards (eleventh tone) were presented to each subject. The loudness of the tones was set in each subject to a comfortable level, which was maintained throughout the experiment.

Data pre-processing and scalp level analysis

Pre-processing and data analysis were performed with SPM8 (<http://www.fil.ion.ucl.ac.uk/spm/>). The data were band-pass filtered between 0.5 and 20 Hz and down-sampled to 200 Hz. A correction for eye movements was performed (for each subject) using the Berg algorithm (S6) as implemented in SPM. The data were then epoched offline, with a peristimulus window of -100 to 400 ms. Artifacts were removed using robust averaging (S4), as described previously (S7). Averaged data were prepared for analysis using a second high-pass filtering at 20Hz and a correction for slow drifts via a third order discrete

cosine transform procedure, as implemented in SPM. Trials were sorted in terms of tone repetition (*S4*). In other words, trials one to eleven corresponded to the responses elicited after one to eleven presentations of the same tone, collapsed across the whole range of frequencies. The first trial in each train (corresponding to the oddball or the deviant) and the eleventh (corresponding to the standard) were retained for further analysis. Data were transformed into scalp-map images (*S4*), which were then entered in a second level between-subjects random effects analysis. This used an ANCOVA model, with stimulus type (standard versus deviant) and the level of consciousness (3 levels: controls, MCS and VS) as factors. The different observations were assumed to be independent but their variances were assumed to be unequal. As previous studies (*S8-9*) show a correlation between mismatch negativity amplitude and prognosis, the patients' prognosis at 1 month were entered as a covariate of no interest (in VS patients: values of -2 if death, -1 if stay VS, 1 if evolution towards MCS; in MCS patients: -1 if stay MCS, 1 if emergence from MCS). F-contrasts were specified to test for differences between deviant and standard in controls, MCS and VS populations (simple effects of trial in each group). Finally, we used an F-contrast to search for the interaction with group; i.e., an ERP amplitude difference attributable to differences in the level of consciousness across the three populations. In all the SPM analyses, results were thresholded at $p\text{-value} < 0.05$, corrected for multiple comparisons using Random Field Theory in the usual way (*S10*). The peak latencies we refer to in the results are those of the local maxima of statistical significance of scalp-time group F-maps, as reported by SPM software.

The Supplementary Fig. shows instantaneous scalp T-maps over time, for the comparison standards versus deviants, in individual MCS and VS patients. These maps were obtained after filtering from 0.5 to 20 Hz, correction for eye movements using the Berg algorithm described above, epoching from -100 to 400 ms, and correction of trials for slow drifts using a third order discrete cosine transform, as implemented in SPM. Individual epoched data were then converted to scalp-time images and a two sample T-test was performed, searching for a differential effect between standards and deviants in each patient. Scalp T-maps are displayed un-thresholded and at $p < 0.001$, uncorrected. In general, MCS patients show more robust differences at the individual level, although we did not obtain significant individual results in all patients. Note that the statistical criterion we used here is more conservative than commonly employed in ERP reports: a p-value threshold of 0.001 is equivalent to a correction for multiple comparisons over 50 time-points. The Supplementary Fig. also displays averaged ERP time courses in each MCS and VS patient. These were used for all our group analyses.

Dynamic causal modeling

Dynamic causal modeling (DCM) was originally developed for connectivity analysis of fMRI (S11) and M/EEG data (S12). Most approaches to connectivity analysis of M/EEG data use functional connectivity measures such as coherence or temporal correlations, which establish statistical dependencies between two time-series. However, there are certain cases where causal interactions are the focus of interest. In these situations, DCM is particularly useful, because it estimates effective connectivity (the influence one neuronal system has over another), under a perturbation, or stimulus. DCM models the interactions among cortical regions and allows one to make inferences about the parameters of that model and investigate how these parameters are influenced by experimental factors. DCM uses generative or forward models for evoked responses as measured with EEG/MEG (S12-13), and provides an important advance over conventional analyses of evoked responses because it places biophysically plausible constraints on the inversion; namely, activity in one source has to be caused by activity in another. DCMs for MEG/EEG use neural mass models (S14) to explain source activity in terms of the ensemble dynamics of interacting inhibitory and excitatory subpopulations of neurons, based on the model of Jansen and Rit (S15). The active sources are interconnected according to the connectivity rules described in (S16) and conform to a hierarchical model of intrinsic and extrinsic connections within and among multiple sources as described in (S17) and (S18). By taking the marginal likelihood over the conditional density of the model parameters, one can estimate the probability of the data, given a particular model. This is known as the marginal likelihood or evidence and can be used to compare and select the best model amongst alternative models. We have previously used DCM to explain ERPs to standards and deviants using a classical (S19) and roving paradigm (S4-5). Differences in the ERP to standards and deviants were modeled in terms of changes in synaptic connections within and between hierarchically organized cortical sources. Model comparison addressed hierarchical implementations of multiple-level network models ranging from one to three levels. These models allowed for changes in extrinsic connections in combination with changes in intrinsic connections at the different levels of the cortical hierarchy.

Model specification

DCM is usually used in a hypothesis-driven fashion: it does not explore all possible models but tests specific mechanistic hypotheses. Our models attempt to explain the generation of each individual response (i.e., responses to each tone presentation). Therefore, left and right A1 were chosen as cortical input stations for processing the auditory information. Doeller et al. (S20) identified sources for the differential response, with fMRI and EEG measures, in both left and right superior temporal gyrus (STG) and inferior frontal gyrus (IFG). Here, we modeled each active source; i.e., each node in the network, with a single equivalent current dipole (ECD) in a conventional electromagnetic forward model. This electromagnetic model used boundary element head models (S21), with homogeneous and isotropic conductivity as an approximation to the brain, cerebrospinal fluid (CSF), skull and scalp surfaces. Subject-specific head models were obtained using an inverse spatial normalization of a canonical mesh for each subject. Normalization parameters were obtained using unified segmentation of the subjects' structural images (computerized tomography or T1 MRI) as implemented in the SPM software. Coregistration of electrode position and head model was performed in each subject, prior to forward model computation. After the forward model was computed for each subject, the lead-field mapping cortical sources onto measured signals was parameterized in terms of the location and orientation of each dipole source in the DCM (S4). The coordinates reported by Opitz et al. (S22) (for STG and IFG) and Rademacher et al. (S23) (for left and right primary auditory cortex, A1) were chosen as prior source location means, with a prior variance of 16mm^2 . We converted these coordinates, given in the literature in Talairach space, to MNI space using the algorithm described in <http://imaging.mrc-cbu.cam.ac.uk/imaging/MniTalairach>. The moment parameters had prior mean of zero and a variance of 256mm^2 in each direction. This is equivalent to assuming uninformative or flat priors on the orientations of the dipole moments. For computational expediency, DCMs (see below) were computed on a reduced form of data that corresponded to eight channel mixtures or spatial modes. These were the eight principal modes of a singular value decomposition (SVD) of the channel data between 0 and 400 ms, over the trial types of interest. These were the standard and deviant trials above.

DCMs

Bayesian model selection considered eleven models specified by their architecture (see Fig. 3). These models covered different levels of hierarchical complexity, both in terms of the number of areas involved, and the extrinsic (between-source) connections. The models started

with the most parsimonious model, Model 1 (a one-level hierarchical model comprising two nodes in the left and right A1) and increased in their complexity, in terms of hierarchical levels, number of sources and extrinsic connections. The inclusion of nodes and connections to the initial model culminated in a non-symmetric three-level hierarchical model that included bilateral A1 and STG, and right IFG. All models can therefore be considered as a sub-model of the last one, Model 11. Our simplest model, Model 1, is a two source network corresponding to the hypothesis that the ERPs are generated by bilateral activity in A1. Models 2 to 5 build on Model 1 through addition of left and right STG sources (connected through forward connections to ipsilateral A1, and in more complex models through backward connections to ipsilateral A1, and/or via lateral connections with each other). A third-level family of models, Models 6 to 11, comprising five sources, included a right IFG source. Right STG was connected with ipsilateral IFG. Models 6 to 11 differ in the successive addition of backward and lateral connections at different levels of the cortical hierarchy. We accommodated differences in the ERP to standard and deviants by condition-specific scaling parameters on every connection in each model. This meant that Models 2 to 11 cover the hypotheses that both local adaptation (*S24*), within each area, and interactions within a temporo-frontal network (*S25-26*) underlie the generation of the MMN.

Statistical analysis

Statistical analyses in this paper were based on a two-stage (summary-statistic) approach. In a first stage, Bayesian model comparison was used to optimize the network architecture (DCM) underlying electrophysiological responses to auditory stimulation in controls, MCS and VS patients. In a second stage, a quantitative connectivity analysis was performed, conditioned upon the winning model, searching for differences in connectivity between controls, MCS and VS patients, in response to auditory stimulation. The second stage used the conditional (within-subject) estimates of effective connections from the winning DCM as the dependent variable in a classical (between-subject) ANOVA.

Bayesian model selection (BMS)

DCM inversion involves optimizing a model (m) which provides two important quantities: the free-energy bound on the model-evidence $p(y|m)$, used for model comparison, and the posterior or conditional density of the model parameters, $p(\theta|y,m)$. Specifically, inversion of a

DCM corresponds to approximating the posterior probability of the parameters using variational Bayes (S27). The aim is to minimize a free-energy bound on the log-evidence, with respect to a variational density, $q(\theta)$. When the free-energy is minimized; $q(\theta)=p(\theta|y,m)$ and the free-energy $F = -\ln p(y|m)$ approximates the negative marginal log-likelihood or negative log-evidence. After convergence, the variational density is used as an approximation to the desired conditional density and the log-evidence is used for model comparison.

One often wants to compare different models and select the best before making statistical inferences on the basis of the conditional density (see above). The best model, given the data, is the one with the highest log-evidence, $\ln p(y|m)$ (assuming a uniform prior over models). Given two models m_1 and m_2 one can compare them by computing their relative log-evidence $\ln p(y|m_1)-\ln p(y|m_2)$ (S4). One may wish to select the model that best explains multiple data sets, i.e., the best model at the group level. Alternatively, we can make inferences about general characteristics of model architecture using family-based inferences, which compare different groups of models characterized by similar architectural properties (S28). We thus performed family-wise inferences in each population, using a random effects approach, which is robust to potential outliers in the population (S29). A first family-wise inference optimized the number of areas that explained the data of the three populations. We separated the model space into three families: two-area models with bilateral A1 only (Model 1); four-area models with bilateral A1 and STG (Models 2 to 5), and five-area models with bilateral A1 and STG, and right IFG (Models 6 to 11). Bayesian model selection showed that the five-area models were the best. A second family-wise inference addressed the connectivity architecture. Three families were considered: models with no inter-areal connections (Model 1), models with forward connections only (Models 2, 5, 6 and 7), and models with both forward and backward connections (Models 3, 4, 8, 9, 10 and 11). This BMS procedure established the presence of recurrent connections, involving the prefrontal source, and demonstrates the consistency of BMS over the three groups of subjects (Fig. 3 – left panel). The superiority of the full model (model 11) was confirmed with an exhaustive model search over all models using a (random effects) BMS over all subjects (Fig. 3 – right panel). Fig. 3 (lower panel) displays source activity estimates in representative subjects according to this model. These predictions of source activity over time illustrate the preservation of frontal responsiveness in MCS as in VS patients.

Quantitative connectivity analysis

We used the winning model above for final (between-subject) statistical analysis of the conditional estimates of connectivity. In our DCMs, the effects of deviant stimuli (relative to standards) are modeled by scaling the effective connectivity in a trial-specific fashion. Although we tested for group differences in this (MMN-related) scaling, our primary interest was in differences in the underlying connection strengths mediated distributed responses to all stimuli. We exported the connectivity estimates to SPSS, and performed an ANCOVA, using the patients' prognosis as a covariate of no interest (as defined above). We tested each forward and backward connection independently with appropriate contrasts. We first searched for an effect of the level of consciousness on changes in connectivity between standard and deviants. We then tested for group differences in connection strength *per se*. We found a significant difference in the backward connection between frontal and temporal cortices between controls, MCS and VS, at $p < 0.05$, corrected for multiple comparisons using Bonferroni procedure; i.e., taking into account the number of connections tested.

Supplementary discussion

Previous literature on MMN in healthy volunteers

There is a large literature validating DCM for electrophysiological responses that uses both psychological (*S4, S18-19, S30-38*) and psychopharmacological (*S39-40*) constructs. The choice of the mismatch negativity paradigm in the current study was based on several years of experience with this paradigm and its modeling (with both DCM (*S4, S18-19, S31-32, S41*) and neuronal simulations (*S18, S42*)). In short, we chose the mismatch negativity paradigm not only because it was particularly appropriate for the patients we studied but because we have a wealth of information about the underlying mechanisms and networks from lesions studies (e.g. (*S43-44*)), fMRI studies of normal subjects (e.g. (*S20, S22, S45*)), high-density EEG (e.g. (*S46-48*)) and MEG studies (e.g. (*S48-50*)). The five area model we used, including a right frontal region (*S22, S46*) has been shown to have the greatest evidence in a number of DCM studies; using different variants of the MMN paradigm and different subjects (*S4, S18-19, S31-32, S41*).

Previous MMN studies in MCS and VS patients

Previous studies have used auditory event-related potentials to assess prognosis in severely brain-damaged patients. The presence of MMN is a good predictor of awakening and suggests that comatose patients will not enter a permanent vegetative state (S8, S51-57). In contrast, only a few studies have investigated the correlation between MMN and level of consciousness. A study by Wijnen and collaborators (S9) showed that the amplitude of the MMN increases with recovery from VS to normal consciousness. This study found a significant correlation between the amplitude of the MMN and level of consciousness, when comparing VS with MCS and subsequent emergence from MCS (S9). A recent study by Fischer and collaborators (S58) failed to replicate these results. However, one might argue that a failure to demonstrate MMN differences does not mean they do not exist (classical statistics control type I, not type II errors). While Wijnen's analysis and our study investigated between-condition differences in MMN amplitude, Fischer et al. used an all-or-none (based on some threshold) MMN scoring procedure in individual brain-damaged patients. Finally, these differences may also speak to the distinction between phenomenological (MMN) differences in observed scalp-level responses (in data-space) and a (possibly more sensitive) comparison of their underlying causes (e.g., coupling strengths – see also discussion below).

Technical comments

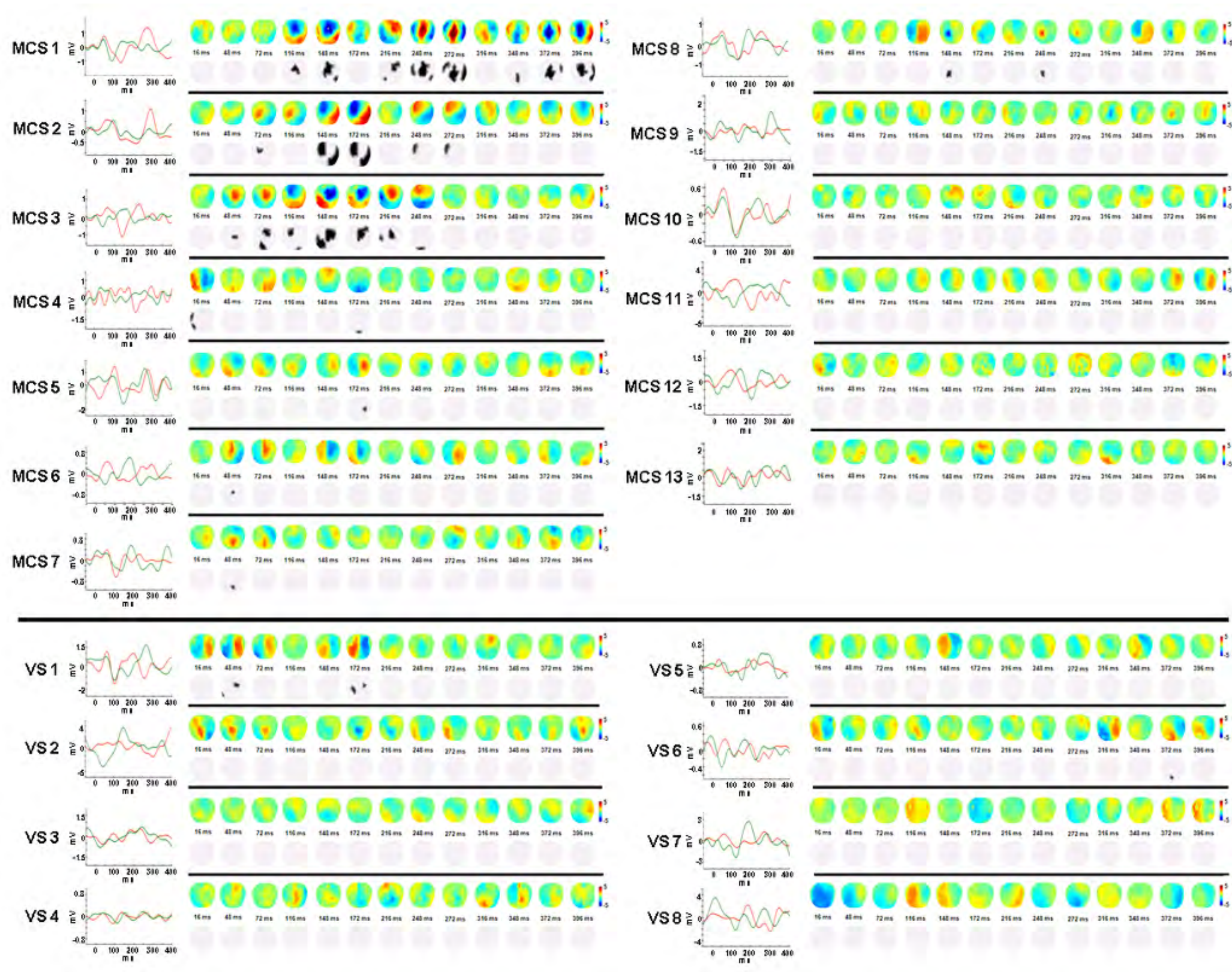
DCM does not examine coupling among sources following the inversion of a classical electromagnetic forward model. It subsumes the inversion of a classical model and tries to explain the data as observed in channel-space. In other words, DCM is a generalization of classical inversion schemes, not an add-on. The parameters estimated from the DCM and the evaluation of the DCMs per se were based on exactly the same (ERP) data. The SPM (scalp-level) analyses report classical inferences on responses over channels and peristimulus time. They represent a statement about phenomena observed in data-space. Conversely, the DCM analyses pertain to the underlying causes of these phenomena and their group differences. These causes include the hidden source activity and coupling parameters. The parameters of the network (DCM) are estimates of the functional architectures producing observed differences. Group comparisons of these parameter estimates (using simple classical inference) allow one to interpret scalp-level differences mechanistically, by appealing to the neurobiologically grounded DCM. Discrepancies between these complementary (SPM and DCM) analyses are resolved easily by noting that a failure to demonstrate a significant difference cannot be taken as evidence for no difference.

It is important to note that the inference about impaired connectivity was direct and based upon simple classical tests (T-tests). This pre-empts any concerns about the robustness or sensitivity of DCM. Put simply, DCM was used to furnish quantities (coupling parameters) that could be interpreted in relation to an underlying model. However, the inference about these quantities was based upon straightforward classical statistics which, under the null hypothesis of no differences, could not have given significant results. The fact that we obtained selective and significant results could be construed as a validation of the DCM; in the sense that it parameterized something that differed significantly between the groups.

At a conceptual level, the model employed here considers the regions involved in the generation of the individual responses in isolation. However, in EEG some nonspecific state variables can have a systematic effect on stimulus processing, and also on the emergence of a conscious experience. An example of this is provided by studies showing that the conscious visual perception depends on the level of occipital alpha (*S59*). Conversely, both sensory stimuli and attention may affect physiological states. In short one cannot ignore interactions among brain state, stimulus processing and conscious awareness. In our patients, the classical EEG markers of brain state were drastically altered. However, it is difficult to be definitive about what causes what. In other words, perceptual processing can cause a change in synaptic coupling, which changes the nature of perceptual processing. A simple example here might be attentional increases in postsynaptic gain (mediated by activity-dependent changes in synaptic efficacy) (*S60*). In our context, this means that a failure of backward connectivity from the frontal region may be a cause or consequence of processing that underlies consciousness. We deliberately chose the mismatch negativity paradigm because it elicits well characterized electrophysiological responses even in the absence of attention and (perhaps) explicit awareness (*S68*). These responses enable us to estimate the underlying network and distributed processing using DCM. However, there is no supposition that the responses elicited in this paradigm are related to the perception of the stimuli used. Associating changes in backward connections from the frontal cortex with conscious perception is based purely upon the fact that it is changes in these and only these connections that are common to patients that show deficits of perceptual awareness. In short, the key experimental manipulation here was not the standard or deviant stimuli of the mismatch negativity paradigm but the selection of subjects with different levels of consciousness. This allowed us to detect changes in network architecture that are related not to the content (perception of a particular sound), but to the level of consciousness. This approach is used in studies correlating the mismatch negativity component with the level of consciousness during

anesthesia (*S61*) and sleep (*S62*). It is also adopted in experiments using transcranial magnetic stimulation (TMS) (*S63-65*): perturbing the system with TMS allows one to characterize network changes underlying various levels of consciousness (*S66-67*). In short, we were able to establish that a failure of backward effective connectivity is associated with decreased level of consciousness. This failure may or may not be necessary to explain any abnormal perceptual content elicited by the standard and oddball stimuli in our paradigm.

Finally, it would be interesting to determine which EEG frequencies contribute to the interactions among sources. In particular, do long-distance backward fronto-temporal connections employ beta-band frequencies or slower (alpha band) or faster dynamics (gamma band)? As fast rhythms like gamma are prone to corruption by non-neuronal noise in scalp-level EEG recordings (*S69*), the use of invasive electrophysiological data may be more suited to answer this question. To address this issue, one could use DCM for induced responses (*S35*). DCM for ERP, as used here, tries to explain evoked as opposed to induced responses. This means that the differences in coupling explain only the evoked data features and do not explain any induced components. It may be that effective connectivity depends upon (or is changed by) high frequency synchronous activity (e.g., communication through coherence or synchronous gain (*S60, S70*)). In a DCM for ERP (as used here) this would be expressed as increased effective connectivity, provided induced responses are expressed consistently in peristimulus time. To understand the relationship between how different data features (e.g., evoked versus induced) are caused one would have to model both explicitly. DCM for induced responses may provide a more rounded picture on what aspects of brain dynamics mediate the coupling between brain regions and the aberrant coupling reported here.



Supplementary Fig. Spatiotemporal differences between standards and deviants in individual MCS and VS. Individual mean ERPs show responses to standard (t_{11} — green) and deviant (t_1 — red) tones at channel Cz (central) for each patient. Scalp plots represent instantaneous Statistical Parametric Maps for differential responses across time. For display purposes, 2D-scalp topographies were interpolated from the 60 channels and results are displayed unthresholded and thresholded at $p < 0.001$ (uncorrected). Color scales correspond respectively to T values and to significant (in black) voxels.

Supplementary Table. Clinical, electrophysiological and structural imaging data of patients.

	MCS1	MCS2	MCS3	MCS4	MCS5	MCS6	MCS7	MCS8	MCS9
Clinical Features									
Sex (age, years)	Male (27)	Male (20)	Male (38)	Male (46)	Female (60)	Male (28)	Male (71)	Female (38)	Male (19)
Cause	Anoxic	Trauma	Anoxic	Trauma	Haemorrhage	Trauma	Stroke	Haemorrhage	Trauma
Time of EEG after insult	1 month	3 years	13 years	27 years	1 month	6 years	18 days	12 days	1 year
Outcome at 1 month	MCS	MCS	MCS	MCS	EMCS	MCS	MCS	MCS	MCS
Paralysis/paresis	Tetraparesis	Tetraparesis	Tetraparesis	Tetraparesis	Right-sided hemiparesis	Tetraparesis	Right-sided hemiparesis	Tetraparesis	Tetraparesis
Coma Recovery Scale-Revised									
Diagnosis at time of EEG	MCS	MCS	MCS	MCS	MCS	MCS	MCS	MCS	MCS
Auditory function	Auditory startle	Auditory startle	None	Reproducible movement to command	Reproducible movement to command	Auditory startle	Localization to sound	Reproducible movement to command	Reproducible movement to command

Visual function	Visual pursuit	Visual pursuit	Visual pursuit	Object recognition	Visual startle	Visual pursuit	Fixation	Visual pursuit	Visual pursuit
Motor function	Flexion withdrawal	Abnormal posturing	Automatic motor response	Automatic motor response	Abnormal posturing	Flexion withdrawal	Automatic motor response	Automatic motor response	Abnormal posturing
Oromotor/Verbal function	None	Oral reflexive movement	Oral reflexive movement	Intelligible verbalization	None	Vocalization/Oral movement	Vocalization/Oral movement	Vocalization/Oral movement	Oral reflexive movement
Communication	Non-Functional: Intentional	Non-Functional: Intentional	None	Non-Functional: Intentional	None	None	None	Non-Functional: Intentional	None
Arousal	Eye opening without stimulation	Eye opening without stimulation	Eye opening without stimulation	Attention	Eye opening with stimulation	Eye opening without stimulation	Eye opening without stimulation	Eye opening without stimulation	Eye opening without stimulation
Total score	9	9	11	21	7	10	13	15	10
EEG									
Background activity	Bilateral slow	Bilateral slow	Bilateral slow	Bilateral slow	Bilateral slow	Bilateral slow	Left hemispheric	Right	Bilateral slow

	theta-delta dysrhythmia	theta-delta dysrhythmia	theta dysrhythmia	theta-delta dysrhythmia	theta-delta dysrhythmia	theta-delta dysrhythmia	theta-delta dysrhythmia	hemispheric theta-delta dysrhythmia	theta-delta dysrhythmia
MRI/CT									
Lesions	Anoxic lesions in bilateral basal ganglia and corticospinal tracts	Diffuse fronto- temporal, thalamic and ponto- mesencephalic atrophy	Diffuse bilateral leuco- encephalopathy	Major bilateral thalamic and cerebral atrophy. External capsule T2 hyperintensity	Bilateral frontal hemorrhagic collections and right ponto- mesencephalic ischemic lesion	Bilateral contusional sequellae in frontal and temporal lobes	Left sylvian territory ischemic lesion	Right subdural haematoma with right hemisphere compression and contusions	Diffuse bilateral leuco- encephalopathy predominant in frontal lobes

Supplementary Table (continued). Clinical, electrophysiological and structural imaging data of patients.

	MCS10	MCS11	MCS12	MCS13
Clinical Features				
Sex (age, years)	Male (32)	Female (48)	Female (54)	Female (62)
Cause	Anoxic	Anoxic	Trauma	Haemorrhage
Time of EEG (after insult)	1 month	2 months	9 years	20 days
Outcome at 1 month	MCS	MCS	MCS	MCS
Paralysis/paresis	Mild tetraparesis	Mild tetraparesis	Tetraparesis	Tetraparesis
Coma Recovery Scale-Revised				
Diagnosis at time of EEG	MCS	MCS	MCS	MCS
Auditory function	Reproducible movement to	Localization to sound	Auditory startle	Auditory startle

	command			
Visual function	Visual pursuit	Visual pursuit	Visual pursuit	Visual pursuit
Motor function	Automatic motor response	Automatic motor response	Flexion withdrawal	Flexion withdrawal
Oromotor/Verbal function	Vocalization/ Oral movement	Vocalization/ Oral movement	None	Oral reflexive movement
Communication	None	Non- Functional: Intentional	None	None
Arousal	Eye opening without stimulation	Eye opening without stimulation	Eye opening with stimulation	Eye opening with stimulation
Total score	15	15	7	8
EEG				
Background activity	Bilateral slow	Bilateral slow	Bilateral slow	Bilateral slow

	theta dysrhythmia	delta dysrhythmia	theta dysrhythmia	theta dysrhythmia
MRI/CT				
Lesions	No acute lesion demonstrated	Bilateral chronic ischemic lesions in cerebral hemispheres	Bilateral frontal contusions and bilateral fronto- parietal leuco- encephalopathy	Bilateral anterior and sylvian haemorrhage With ventricular inondation

Supplementary Table (continued). Clinical, electrophysiological and structural imaging data of patients.

	VS1	VS2	VS3	VS4	VS5	VS6	VS7	VS8
Clinical Features								
Sex (age, years)	Male (67)	Male (16)	Female (77)	Male (43)	Female (83)	Male (34)	Female (60)	Female (60)
Cause	Anoxic	Trauma	Haemorrhage	Anoxic	Trauma	Anoxic	Haemorrhage	Haemorrhage
Time of EEG (days after insult)	9 months	12 days	14 days	22 days	1 month	21 years	15 days	1 month
Outcome at 1 month	VS	EMCS	VS	VS	Death	VS	EMCS	EMCS
Paralysis/paresis	Tetraparesis	Tetraparesis	Tetraparesis	Tetraparesis	Tetraparesis	Tetraparesis	Tetraparesis	Tetraparesis
Coma Recovery Scale- Revised								
Diagnosis at time of EEG	VS	VS	VS	VS	VS	VS	VS	VS
Auditory function	None	None	None	None	None	Auditory startle	None	None
Visual function	None	None	None	None	None	Visual startle	None	None

Motor function	Abnormal posturing	Flexion withdrawal	Abnormal posturing	Flexion withdrawal	None	Abnormal posturing	Flexion withdrawal	Abnormal posturing
Oromotor/Verbal function	None	None	Oral reflexive movement	Oral reflexive movement	Oral reflexive movement	Vocalization/ Oral movement	Vocalization/ Oral movement	Oral reflexive movement
Communication	None	None	None	None	None	None	None	None
Arousal	Eye opening without stimulation	Eye opening with stimulation	Eye opening with stimulation	Eye opening with stimulation	Eye opening with stimulation	Eye opening without stimulation	Eye opening with stimulation	Eye opening with stimulation
Total score	3	3	3	4	2	7	5	3
EEG								
Background activity	Bilateral slow theta dysrhythmia	Bilateral slow theta-delta dysrhythmia	Bilateral slow theta-delta dysrhythmia	Bilateral slow theta dysrhythmia	Bilateral slow theta-delta dysrhythmia	Bilateral slow theta dysrhythmia	Bilateral slow theta-delta dysrhythmia	Bilateral slow theta-delta dysrhythmia
MRI/CT								
Lesions	Right fronto-parietal	Left occipital and right	Bilateral sylvian	Bilateral insular, basal	Bilateral frontal	Major bilateral cerebral and	Left fronto-temporo-	Intraventricular haemorrhage

	hypoxic lesion	temporal and cerebellar peduncle contusion	territory ischemic lesions	ganglia and thalamic ischemic lesions	contusions and fronto-temporo-parietal haematoma	cerebellar atrophy	parietal stroke with secondary haemorrhage involving thalamus and brainstem	secondary to basilar aneurysm rupture
--	----------------	--	----------------------------	---------------------------------------	--	--------------------	---	---------------------------------------

References

- S1. J. T. Giacino, K. Kalmar, J. Whyte, The JFK Coma Recovery Scale-Revised: measurement characteristics and diagnostic utility. *Archives of physical medicine and rehabilitation* **85**, 2020 (Dec, 2004).
- S2. R. T. Seel *et al.*, Assessment scales for disorders of consciousness: evidence-based recommendations for clinical practice and research. *Arch Phys Med Rehabil* **91**, 1795 (Dec, 2010).
- S3. J. Virtanen, J. Ruohonen, R. Naatanen, R. J. Ilmoniemi, Instrumentation for the measurement of electric brain responses to transcranial magnetic stimulation. *Medical & biological engineering & computing* **37**, 322 (May, 1999).
- S4. M. I. Garrido *et al.*, The functional anatomy of the MMN: a DCM study of the roving paradigm. *Neuroimage* **42**, 936 (Aug 15, 2008).
- S5. M. I. Garrido *et al.*, Repetition suppression and plasticity in the human brain. *Neuroimage* **48**, 269 (Oct 15, 2009).
- S6. P. Berg, M. Scherg, A multiple source approach to the correction of eye artifacts. *Electroencephalogr Clin Neurophysiol* **90**, 229 (Mar, 1994).
- S7. T. D. Wager, M. C. Keller, S. C. Lacey, J. Jonides, Increased sensitivity in neuroimaging analyses using robust regression. *Neuroimage* **26**, 99 (May 15, 2005).
- S8. C. Fischer, J. Luaute, P. Adeleine, D. Morlet, Predictive value of sensory and cognitive evoked potentials for awakening from coma. *Neurology* **63**, 669 (Aug 24, 2004).
- S9. V. J. Wijnen, G. J. van Boxtel, H. J. Eilander, B. de Gelder, Mismatch negativity predicts recovery from the vegetative state. *Clin Neurophysiol* **118**, 597 (Mar, 2007).
- S10. J. Kilner, K. J. Friston, Topological inference for EEG and MEG. *Ann. Appl. Stat.* **4**, 1272 (2010).
- S11. K. J. Friston, L. Harrison, W. Penny, Dynamic causal modelling. *Neuroimage* **19**, 1273 (Aug, 2003).
- S12. O. David *et al.*, Dynamic causal modeling of evoked responses in EEG and MEG. *Neuroimage* **30**, 1255 (May 1, 2006).
- S13. S. J. Kiebel, O. David, K. J. Friston, Dynamic causal modelling of evoked responses in EEG/MEG with lead field parameterization. *Neuroimage* **30**, 1273 (May 1, 2006).
- S14. O. David, K. J. Friston, A neural mass model for MEG/EEG: coupling and neuronal dynamics. *Neuroimage* **20**, 1743 (Nov, 2003).

- S15. B. H. Jansen, V. G. Rit, Electroencephalogram and visual evoked potential generation in a mathematical model of coupled cortical columns. *Biol Cybern* **73**, 357 (Sep, 1995).
- S16. D. J. Felleman, D. C. Van Essen, Distributed hierarchical processing in the primate cerebral cortex. *Cereb Cortex* **1**, 1 (Jan-Feb, 1991).
- S17. O. David, L. Harrison, K. J. Friston, Modelling event-related responses in the brain. *Neuroimage* **25**, 756 (Apr 15, 2005).
- S18. S. J. Kiebel, M. I. Garrido, K. J. Friston, Dynamic causal modelling of evoked responses: the role of intrinsic connections. *Neuroimage* **36**, 332 (Jun, 2007).
- S19. M. I. Garrido, J. M. Kilner, S. J. Kiebel, K. J. Friston, Evoked brain responses are generated by feedback loops. *Proc Natl Acad Sci U S A* **104**, 20961 (Dec 26, 2007).
- S20. C. F. Doeller *et al.*, Prefrontal cortex involvement in preattentive auditory deviance detection: neuroimaging and electrophysiological evidence. *Neuroimage* **20**, 1270 (Oct, 2003).
- S21. M. Fuchs, M. Wagner, J. Kastner, Boundary element method volume conductor models for EEG source reconstruction. *Clin Neurophysiol* **112**, 1400 (Aug, 2001).
- S22. B. Opitz, T. Rinne, A. Mecklinger, D. Y. von Cramon, E. Schroger, Differential contribution of frontal and temporal cortices to auditory change detection: fMRI and ERP results. *Neuroimage* **15**, 167 (Jan, 2002).
- S23. J. Rademacher *et al.*, Probabilistic mapping and volume measurement of human primary auditory cortex. *Neuroimage* **13**, 669 (Apr, 2001).
- S24. I. P. Jaaskelainen *et al.*, Human posterior auditory cortex gates novel sounds to consciousness. *Proc Natl Acad Sci U S A* **101**, 6809 (Apr 27, 2004).
- S25. I. Winkler, G. Karmos, R. Naatanen, Adaptive modeling of the unattended acoustic environment reflected in the mismatch negativity event-related potential. *Brain Res* **742**, 239 (Dec 2, 1996).
- S26. R. Naatanen, *Attention and Brain Function*. (Lawrence Erlbaum, Hillsdale, New Jersey, 1992).
- S27. K. J. Friston *et al.*, Classical and Bayesian inference in neuroimaging: theory. *Neuroimage* **16**, 465 (Jun, 2002).
- S28. W. D. Penny *et al.*, Comparing families of dynamic causal models. *PLoS computational biology* **6**, e1000709 (Mar, 2010).
- S29. K. E. Stephan, W. D. Penny, J. Daunizeau, R. J. Moran, K. J. Friston, Bayesian model selection for group studies. *Neuroimage* **46**, 1004 (Jul 15, 2009).

- S30. S. J. Kiebel, M. I. Garrido, R. J. Moran, K. J. Friston, Dynamic causal modelling for EEG and MEG. *Cogn Neurodyn* **2**, 121 (Jun, 2008).
- S31. M. I. Garrido, J. M. Kilner, S. J. Kiebel, K. E. Stephan, K. J. Friston, Dynamic causal modelling of evoked potentials: a reproducibility study. *Neuroimage* **36**, 571 (Jul 1, 2007).
- S32. M. I. Garrido, J. M. Kilner, S. J. Kiebel, K. J. Friston, Dynamic causal modeling of the response to frequency deviants. *J Neurophysiol* **101**, 2620 (May, 2009).
- S33. R. J. Moran *et al.*, Dynamic causal models of steady-state responses. *Neuroimage* **44**, 796 (Feb 1, 2009).
- S34. R. J. Moran, K. E. Stephan, R. J. Dolan, K. J. Friston, Consistent spectral predictors for dynamic causal models of steady-state responses. *Neuroimage*, (Jan 13, 2011).
- S35. C. C. Chen, S. J. Kiebel, K. J. Friston, Dynamic causal modelling of induced responses. *Neuroimage* **41**, 1293 (Jul 15, 2008).
- S36. W. D. Penny, V. Litvak, L. Fuentemilla, E. Duzel, K. Friston, Dynamic Causal Models for phase coupling. *J Neurosci Methods* **183**, 19 (Sep 30, 2009).
- S37. J. Daunizeau, S. J. Kiebel, K. J. Friston, Dynamic causal modelling of distributed electromagnetic responses. *Neuroimage* **47**, 590 (Aug 15, 2009).
- S38. M. Fastenrath, K. J. Friston, S. J. Kiebel, Dynamical causal modelling for M/EEG: spatial and temporal symmetry constraints. *Neuroimage* **44**, 154 (Jan 1, 2009).
- S39. R. J. Moran *et al.*, A neural mass model of spectral responses in electrophysiology. *Neuroimage* **37**, 706 (Sep 1, 2007).
- S40. R. J. Moran *et al.*, Bayesian estimation of synaptic physiology from the spectral responses of neural masses. *Neuroimage* **42**, 272 (Aug 1, 2008).
- S41. M. I. Garrido, J. M. Kilner, K. E. Stephan, K. J. Friston, The mismatch negativity: a review of underlying mechanisms. *Clin Neurophysiol* **120**, 453 (Mar, 2009).
- S42. A. C. Marreiros, S. J. Kiebel, K. J. Friston, A dynamic causal model study of neuronal population dynamics. *Neuroimage* **51**, 91 (May 15, 2010).
- S43. C. Alain, D. L. Woods, R. T. Knight, A distributed cortical network for auditory sensory memory in humans. *Brain Res* **812**, 23 (Nov 23, 1998).
- S44. K. Alho, D. L. Woods, A. Algazi, R. T. Knight, R. Naatanen, Lesions of frontal cortex diminish the auditory mismatch negativity. *Electroencephalogr Clin Neurophysiol* **91**, 353 (Nov, 1994).

- S45. S. Molholm, A. Martinez, W. Ritter, D. C. Javitt, J. J. Foxe, The neural circuitry of pre-attentive auditory change-detection: an fMRI study of pitch and duration mismatch negativity generators. *Cereb Cortex* **15**, 545 (May, 2005).
- S46. J. Marco-Pallares, C. Grau, G. Ruffini, Combined ICA-LORETA analysis of mismatch negativity. *Neuroimage* **25**, 471 (Apr 1, 2005).
- S47. L. Fuentemilla, J. Marco-Pallares, T. F. Munte, C. Grau, Theta EEG oscillatory activity and auditory change detection. *Brain Res* **1220**, 93 (Jul 18, 2008).
- S48. T. Rinne, K. Alho, R. J. Ilmoniemi, J. Virtanen, R. Naatanen, Separate time behaviors of the temporal and frontal mismatch negativity sources. *Neuroimage* **12**, 14 (Jul, 2000).
- S49. W. Y. Hsu *et al.*, Memory-based mismatch response to changes in duration of auditory stimuli: an MEG study. *Clin Neurophysiol* **121**, 1744 (Oct, 2010).
- S50. F. J. Hsiao, Z. A. Wu, L. T. Ho, Y. Y. Lin, Theta oscillation during auditory change detection: An MEG study. *Biol Psychol* **81**, 58 (Apr, 2009).
- S51. J. Daltrozzo, N. Wioland, V. Mutschler, B. Kotchoubey, Predicting coma and other low responsive patients outcome using event-related brain potentials: a meta-analysis. *Clin Neurophysiol* **118**, 606 (Mar, 2007).
- S52. C. Fischer *et al.*, Mismatch negativity and late auditory evoked potentials in comatose patients. *Clin Neurophysiol* **110**, 1601 (Sep, 1999).
- S53. C. Fischer *et al.*, Improved prediction of awakening or nonawakening from severe anoxic coma using tree-based classification analysis. *Crit Care Med* **34**, 1520 (May, 2006).
- S54. J. Luaute *et al.*, Late auditory and event-related potentials can be useful to predict good functional outcome after coma. *Arch Phys Med Rehabil* **86**, 917 (May, 2005).
- S55. N. M. Kane, S. H. Curry, S. R. Butler, B. H. Cummins, Electrophysiological indicator of awakening from coma. *Lancet* **341**, 688 (Mar 13, 1993).
- S56. N. M. Kane *et al.*, Event-related potentials--neurophysiological tools for predicting emergence and early outcome from traumatic coma. *Intensive Care Med* **22**, 39 (Jan, 1996).
- S57. L. Naccache, L. Puybasset, R. Gaillard, E. Serve, J. C. Willer, Auditory mismatch negativity is a good predictor of awakening in comatose patients: a fast and reliable procedure. *Clin Neurophysiol* **116**, 988 (Apr, 2005).

- S58. C. Fischer, J. Luaute, D. Morlet, Event-related potentials (MMN and novelty P3) in permanent vegetative or minimally conscious states. *Clin Neurophysiol* **121**, 1032 (Jul, 2010).
- S59. G. Thut, A. Nietzel, S. A. Brandt, A. Pascual-Leone, Alpha-band electroencephalographic activity over occipital cortex indexes visuospatial attention bias and predicts visual target detection. *J Neurosci* **26**, 9494 (Sep 13, 2006).
- S60. K. Friston, The free-energy principle: a unified brain theory? *Nat Rev Neurosci* **11**, 127 (Feb, 2010).
- S61. W. Heinke *et al.*, Sequential effects of increasing propofol sedation on frontal and temporal cortices as indexed by auditory event-related potentials. *Anesthesiology* **100**, 617 (Mar, 2004).
- S62. P. Ruby, A. Caclin, S. Boulet, C. Delpuech, D. Morlet, Odd sound processing in the sleeping brain. *J Cogn Neurosci* **20**, 296 (Feb, 2008).
- S63. M. Massimini *et al.*, Breakdown of cortical effective connectivity during sleep. *Science* **309**, 2228 (Sep 30, 2005).
- S64. M. Massimini *et al.*, Cortical reactivity and effective connectivity during REM sleep in humans. *Cogn Neurosci* **1**, 176 (Sep, 2010).
- S65. F. Ferrarelli *et al.*, Breakdown in cortical effective connectivity during midazolam-induced loss of consciousness. *Proc Natl Acad Sci U S A* **107**, 2681 (Feb 9, 2010).
- S66. M. Massimini, M. Boly, A. Casali, M. Rosanova, G. Tononi, A perturbational approach for evaluating the brain's capacity for consciousness. *Prog Brain Res* **177**, 201 (2009).
- S67. M. T. Alkire, A. G. Hudetz, G. Tononi, Consciousness and anesthesia. *Science* **322**, 876 (Nov 7, 2008).
- S68. R. Naatanen, P. Paavilainen, T. Rinne, K. Alho, The mismatch negativity (MMN) in basic research of central auditory processing: a review. *Clin Neurophysiol* **118**, 2544 (Dec, 2007).
- S69. E. M. Whitham *et al.*, Scalp electrical recording during paralysis: quantitative evidence that EEG frequencies above 20 Hz are contaminated by EMG. *Clin Neurophysiol* **118**, 1877 (Aug, 2007).
- S70. P. Fries, A mechanism for cognitive dynamics: neuronal communication through neuronal coherence. *Trends Cogn Sci* **9**, 474 (Oct, 2005).